Stable, entropy-consistent, and localized artificial-viscosity method for capturing shocks and contact discontinuities

By S. S. Jain AND P. Moin

1. Motivation and objectives

Simulations of high-Mach-number compressible flows, and for high Reynolds numbers, require an accurate and stable discontinuity-capturing method. In this work, we propose a novel, entropy-consistent, and stable localized artificial-viscosity/diffusivity (LAD)-based method for capturing shock and contact discontinuities in compressible flows.

Using an analogy between the Lax-Friedrichs (LF) flux and the artificial-viscosity methods, a discrete LF-type flux formulation is proposed for the LAD method. The proposed method satisfies the discrete kinetic energy– and entropy-consistency conditions presented by Jain & Moin (2020), hence the name entropy-consistent localized artificial diffusivity (EC-LAD). We also propose new sensors that localize where the artificial viscosity is acting, and show that the proposed method is suitable for large-eddy simulation (LES) of compressible turbulent flows with shocks. The sensors are designed in a way that the resulting method does not require tuning coefficients, depending on the problem being solved, that are typical of LAD methods. At the end, the extension of the proposed method to compressible two-phase flows is also presented.

2. LAD formulation

The idea behind a LAD method is to add grid-dependent artificial fluid properties to the physical properties locally, in the regions of the flow where discontinuities such as shocks, contacts, and eddies are not resolved by the grid (Cook 2007). The artificial-fluid properties can be summarized as follows.

2.1. *Artificial bulk viscosity*

Here, an artificial bulk viscosity (ABV), β^*, is appended to the physical bulk viscosity, β_p, as

$$\beta = \beta_p + \beta^*, \tag{2.1}$$

and is used to capture shocks on the grid. Initially, a strain-rate-based sensor was used to detect shocks (Cook 2007), but this made the ABV active in regions away from shocks and in turbulent flows. Because shocks are associated with high values of negative dilatation, to reduce the ABV away from shocks, Bhagatwala & Lele (2009) and Mani *et al.* (2009) proposed a dilatation-based sensor. Further, Kawai *et al.* (2010) appended the Ducros sensor (Ducros *et al.* 1999) to the ABV to localize the regions where this is active and to reduce the ABV in the regions of high enstrophy that represent turbulent motions.

2.2. *Artificial shear viscosity*

Here, an artificial shear viscosity (ASV), μ^*, is appended to the physical shear viscosity, μ_p, as

$$\mu = \mu_p + \mu^*, \tag{2.2}$$

and is used as a subgrid model for unresolved eddies. Typically, the magnitude of the strain rate tensor is used as a sensor (Cook 2007).

2.3. *Artificial thermal/mass diffusivity*

Here, an artificial thermal diffusivity (ATD), κ^*, is appended to the physical thermal diffusivity, κ_p, as

$$\kappa = \kappa_p + \kappa^*, \tag{2.3}$$

and is used to capture unresolved contact discontinuities (Cook 2007; Kawai *et al.* 2010; Jain *et al.* 2021). Alternatively, artificial mass diffusivity (AMD), D^*, can be used in the place of ATD (Haga & Kawai 2019) where artificial terms such as $\vec{\nabla} \cdot (D^* \vec{\nabla} \rho)$, $\vec{\nabla} \cdot (D^* \vec{\nabla} \rho \otimes \vec{u})$, and $\vec{\nabla} \cdot \{(|\vec{u}|^2/2) D^* \vec{\nabla} \rho\}$ are consistently added to the mass, momentum, and energy equations.

2.4. *Challenges with the existing methods*

A characteristic of these LAD methods is that they have been most commonly used with high-order numerical methods (Cook 2007; Mani *et al.* 2009; Kawai & Lele 2008; Kawai *et al.* 2010; Lee & Lele 2017; Aslani & Regele 2018; Subramaniam *et al.* 2018; Adler & Lele 2019; Jain *et al.* 2021), with some exceptions (Chandrashekar 2013; Haga & Kawai 2019). However, some of these formulations are too dissipative because of lack of proper localization, and hence are not suitable for the simulation of turbulent flows, and others are less dissipative but do not add enough dissipation locally to resolve the jumps and results in inaccurate capturing of discontinuities. Some formulations are also not stable for high-Reynolds-number flows and require low-pass filters to eliminate oscillations, particularly with high-order numerical methods. Typically, these filters are used in the hope of achieving a stable method; however, the use of low-pass filtering might not necessarily always bring numerical stability to the method. Moreover, the sensors used in the existing formulations require additional Gaussian filtering to achieve a stable method; it is not trivial to extend this filtering operation to unstructured grids for simulations in complex geometries. Additionally, the coefficients in the sensors are known to require problem-dependent tuning. The EC-LAD method proposed in this work aims to address these challenges with existing LAD methods.

3. Proposed artificial-viscosity method

The system of conservation equations (mass, momentum, and energy) along with the proposed artificial-viscosity method can be written as

$$\frac{\partial \rho}{\partial t} + \frac{\partial \rho u_j}{\partial x_j} = A_\rho, \tag{3.1}$$

$$\frac{\partial \rho u_i}{\partial t} + \frac{\partial \rho u_i u_j}{\partial x_j} + \frac{\partial p}{\partial x_i} = \frac{\partial \tau_{ij}}{\partial x_j} + \rho g_i + A_{\rho u}, \tag{3.2}$$

and

$$\frac{\partial E}{\partial t} + \frac{\partial \left(E+p\right) u_j}{\partial x_j} = \frac{\partial \tau_{ij} u_i}{\partial x_j} + \rho u_i g_i + A_E, \tag{3.3}$$

where ρ is the density, p is the pressure, u is the velocity, $E = \rho(e + u_i u_i/2)$ is the total energy and e is the internal energy, τ_{ij} is the stress tensor, and g_i represents a generic body force. Throughout this brief, i and j represent Einstein indices, and x and t represent space and time coordinates, respectively. In Eqs. (3.1)-(3.3), A_ρ, $A_{\rho u}$, and A_E are the artificial terms added to the mass, momentum, and energy equations, respectively, to capture shocks and contact discontinuities. They can be written as

$$A_\rho = \frac{\partial}{\partial x_j}\left(D^* \frac{\partial \rho}{\partial x_j}\right), \tag{3.4}$$

$$A_{\rho u} = \frac{\partial}{\partial x_j}\left(D^* u_i \frac{\partial \rho}{\partial x_j}\right) + \frac{\partial}{\partial x_j}\left(\beta^* \frac{\partial u_k}{\partial x_k}\delta_{ij}\right), \tag{3.5}$$

and

$$A_E = \frac{\partial}{\partial x_j}\left[D^* \frac{\partial \rho}{\partial x_j}\left(\frac{u_k u_k}{2}\right)\right] + \frac{\partial}{\partial x_j}\left(D^* \frac{\partial \rho e}{\partial x_j}\right) + \frac{\partial}{\partial x_j}\left(\beta^* \frac{\partial u_k}{\partial x_k}\delta_{ij} u_i\right). \tag{3.6}$$

Here, Eq. (3.4), the first term in Eq. (3.5), and the first two terms in Eq. (3.6) are added to capture contact discontinuities; and the second term in Eq. (3.5) and the last term in Eq. (3.6) are added to capture shocks. These consistent terms in the momentum and energy equations can be derived similarly to the derivation of interface-regularization terms described by Jain *et al.* (2020). The consistent terms in the momentum and energy equations are introduced such that there is no spurious contribution to the total kinetic energy of the system. Note that, in this work, the ASV is not used. Instead, a dynamic subgrid-scale eddy viscosity model will be adopted in the future (Germano *et al.* 1991).

The artificial diffusivities used in this work can be defined as

$$D^* = C_D \frac{1}{\rho}\left|\sum_j \frac{\partial^r \rho}{\partial x_j^r}(\Delta x_j)^{r+1}\right|\left(|\bar{u}_j^{(m\pm\frac{1}{2})}| + c_s\right) f_D, \tag{3.7}$$

and

$$\beta^* = C_\beta \rho \left|\sum_j \frac{\partial^r \theta}{\partial x_j^r}(\Delta x_j)^{r+2}\right| H(-\theta) f_\beta, \tag{3.8}$$

where m is the grid index; Δx is the grid size; the overbar $\bar{\cdot}^{(m\pm1/2)}$ denotes an arithmetic average of a quantity at m and $m\pm1$; C_D and C_β are the coefficients for AMD and ABV, respectively; c_s is the speed of sound; $\theta = \vec{\nabla}\cdot\vec{u}$ is the dilatation; and f_D and f_β are the switching sensors defined as

$$f_D = \left[\frac{|\frac{\partial \rho}{\partial x_j}|^2}{|\frac{\partial \rho}{\partial x_j}|^2 + a(\theta^2 + \omega_i\omega_i)\left(\frac{\rho}{|\vec{u}|}\right)^2 + \varepsilon}\right], \tag{3.9}$$

and

$$f_\beta = \left(\frac{\theta^2}{\theta^2 + a\omega_i\omega_i + \varepsilon}\right), \tag{3.10}$$

respectively. Here, f_β is a modified version ($a > 1$) of the original Ducros sensor (Ducros

et al. 1999) that was used by Kawai *et al.* (2010) to localize ABV for capturing shocks; and f_D is a new sensor that we propose to localize AMD for capturing contact discontinuities. The purpose of adding this new sensor f_D is to localize AMD further by making it active in the regions containing contact discontinuities and to turn off AMD in the regions with high enstrophy and high dilatation, which represent vortical motions and shocks, respectively. Note that the proposed f_D can also be used with an ATD for capturing contact discontinuities without loss of generality, and we have verified that the advantages of using f_D with AMD also carry over to ATD (results not included here).

Furthermore, in this study, a value of $r = 1$ is used. Note that a higher value of r was used in other studies that use higher-order schemes (Cook 2007; Mani *et al.* 2009; Kawai & Lele 2008; Kawai *et al.* 2010; Lee & Lele 2017; Aslani & Regele 2018; Subramaniam *et al.* 2018; Adler & Lele 2019; Jain *et al.* 2021). In previous studies, a higher value of r was suggested because it results in dissipating only the higher-wavenumber content that is not resolved by the scheme. However, in this study, with the use of a low-order scheme, the motivation to use $r = 1$ (a lower value of r) is to have a sensor that is more localized only at the discontinuities and not to dissipate unresolved scales, unlike the motivation for higher-order schemes. For lower-order schemes, a higher value of $r > 2$ makes the sensor active in other regions in the domain where there is no shock or a contact discontinuity, and this would not be ideal for the simulation of turbulent flows.

3.1. *Problem-independent coefficients*

The coefficients C_D and C_β are generally dependent on the numerical scheme used. In this work, for the second-order central schemes, we use the values $C_D \approx 0.5$, $C_\beta \approx 100$, and $a \approx 100$. Note that the results are fairly robust to these values and do not change with a change in values of these coefficients, as long as those values are changed by less than an order of magnitude. We also show that these coefficients are not dependent on the problem being solved, primarily due to the use of sophisticated sensors in Eqs. (3.9) and (3.10) that are responsible for adding dissipation locally only in the regions where it is needed the most. Hence, the values of these coefficients C_D and C_β need to be determined only once for a particular scheme.

4. Discrete kinetic energy– and entropy-consistent dissipative flux formulation

We first show an analogy between the LF flux and the artificial-viscosity methods, and then use this idea to develop kinetic energy– and entropy-consistent flux formulations for the proposed artificial-viscosity method. Consider a general conservation equation of the form

$$\frac{\partial \phi}{\partial t} + \frac{\partial f(\phi)}{\partial x} = 0, \tag{4.1}$$

where ϕ is a conserved quantity, and $f(\phi)$ is the flux function. Using the explicit Euler (EE) time-advancement scheme and the second-order central scheme, the discrete form of the equation can be written as

$$\phi_m^{n+1} = \phi_m^n - \frac{\Delta t}{2\Delta x}\left[f(\phi_{m+1}^n) - f(\phi_{m-1}^n)\right].$$

Now, replacing ϕ_m^n with $(\phi_{m+1}^n + \phi_m^n)/2$, and rewriting in conservation (flux) form, we obtain

$$\phi_m^{n+1} = \phi_m^n - \lambda\left(\hat{f}_{m+\frac{1}{2}} - \hat{f}_{m-\frac{1}{2}}\right),$$

where the numerical flux, $\hat{f}_{m+1/2}$, is the well known LF flux (LeVeque 1992), given by

$$\hat{f}_{m+\frac{1}{2}} = \left[\frac{f(\phi^n_{m+1}) + f(\phi^n_{m-1})}{2}\right] - \frac{1}{2\lambda}(\phi^n_{m+1} - \phi^n_m), \tag{4.2}$$

and $\lambda = \Delta t/\Delta x$ has units of inverse velocity. Now consider the same conservation equation in Eq. (4.1) with a generic artificial-viscosity fluid property, ϵ^*,

$$\frac{\partial \phi}{\partial t} + \frac{\partial f(\phi)}{\partial x} = \frac{\partial}{\partial x}\left[\epsilon^* \frac{\partial \phi}{\partial x}\right].$$

Using EE and second-order central schemes and writing in conservation form, we arrive at

$$\phi^{n+1}_m = \phi^n_m - \lambda\left[\hat{f}_{m+\frac{1}{2}} - \hat{f}_{m-\frac{1}{2}}\right],$$

where the numerical flux is

$$\hat{f}_{m+\frac{1}{2}} = \left[\frac{f(\phi^n_{m+1}) + f(\phi^n_{m-1})}{2}\right] - \frac{\epsilon^*_{m+\frac{1}{2}}}{\Delta x}(\phi^n_{m+1} - \phi^n_m). \tag{4.3}$$

Note that if $\epsilon^* = 2\Delta x/\lambda$, then the LF flux and the artificial-viscosity method are identical (provided that a second-order central scheme is used for the discretization of the artificial-viscosity terms).

The LF flux is known to be entropy stable, but it is also highly dissipative. Therefore, the idea proposed in this work is to replace the non-dissipative central-flux in the LF flux with a kinetic energy– and entropy-preserving (KEEP) flux in Jain & Moin (2020) and to further localize the dissipative part of the LF flux, only to those regions where they are needed, with the use of sensors. The new proposed flux can then be represented as

$$\hat{f}_{m+\frac{1}{2}} = \hat{f}_{m+\frac{1}{2}}\Big|_{KEEP} - \hat{f}^d_{m+\frac{1}{2}}, \tag{4.4}$$

where $\hat{f}^d_{m+1/2}$ is the dissipative flux given by

$$\hat{f}^d_{m+\frac{1}{2}} = \frac{\epsilon^*_{m+\frac{1}{2}}}{\Delta x}\left(\phi^{n+1}_{m+1} - \phi^n_m\right). \tag{4.5}$$

Here, $\epsilon^*_{m+1/2}$ represents a localized artificial-fluid property. In this work, the non-dissipative central flux is replaced with the second-order KEEP scheme of Jain & Moin (2020). However, in general, this central flux can be replaced with any other low/non-dissipative flux.

Chandrashekar (2013) explored a similar idea by replacing the non-dissipative central flux with a kinetic energy-preserving (KEP) flux. But the dissipative flux in their approach was not localized and was present everywhere in the domain. Another difference is that they used a scalar dissipation of momentum to capture all discontinuities. The scalar dissipation of momentum not only acts on the dilatational motion at the shocks, but also dissipates the vortical structures, which makes the method even more dissipative and unsuitable for the simulation of turbulent flows. They concluded that this approach was too dissipative.

5. Discrete fluxes for the proposed method

The discrete consistency conditions between the mass, momentum, kinetic energy, and internal energy convective fluxes proposed by Jain & Moin (2020) can be further extended

to include dissipative fluxes. If the full mass flux is written as

$$\hat{C}_j^f|_{(m\pm\frac{1}{2})} = \hat{C}_j|_{(m\pm\frac{1}{2})} + \hat{C}_j^{'}|_{(m\pm\frac{1}{2})}, \tag{5.1}$$

where $\hat{C}_j|_{(m\pm1/2)}$ is the convective part and $\hat{C}_j^{'}|_{(m\pm1/2)}$ is the dissipative part, then, the momentum- and kinetic energy–consistency conditions are given by

$$\hat{M}_{ij}^f|_{(m\pm\frac{1}{2})} = \left(\hat{C}_j|_{(m\pm\frac{1}{2})} + \hat{C}_j^{'}|_{(m\pm\frac{1}{2})}\right)\bar{u}_i^{(m\pm\frac{1}{2})} + \hat{M}_{ij}^{'}|_{(m\pm\frac{1}{2})}, \tag{5.2}$$

and

$$\hat{K}_j^f|_{(m\pm\frac{1}{2})} = \left(\hat{C}_j|_{(m\pm\frac{1}{2})} + \hat{C}_j^{'}|_{(m\pm\frac{1}{2})}\right)\frac{u_i|_{(m\pm1)}u_i|_{(m)}}{2} + \bar{u}_i^{(m\pm\frac{1}{2})}\hat{M}_{ij}^{'}|_{(m\pm\frac{1}{2})}, \tag{5.3}$$

where $\hat{M}_{ij}^{'}|_{(m\pm1/2)}$ represents an additional momentum dissipative flux. Using these consistency conditions, and following the notation used in Eq. (4.5) for the LF-type dissipative fluxes, the proposed artificial-viscosity method—an EC-LAD method—can be written in discrete flux form as

$$\hat{C}_j^d|_{(m\pm\frac{1}{2})} = -\frac{D^*_{m\pm\frac{1}{2}}}{\Delta x_j}(\Delta_j\rho), \tag{5.4}$$

$$\hat{M}_{ij}^d|_{(m\pm\frac{1}{2})} = \left(-\frac{D^*_{m\pm\frac{1}{2}}}{\Delta x_j}(\Delta_j\rho)\right)\bar{u}_i^{(m\pm\frac{1}{2})} - \beta^*_{m\pm\frac{1}{2}}\widehat{\frac{\partial u_k}{\partial x_k}}|_{(m\pm\frac{1}{2})}\delta_{ij}, \tag{5.5}$$

$$\hat{K}_j^d|_{(m\pm\frac{1}{2})} = \left(-\frac{D^*_{m\pm\frac{1}{2}}}{\Delta x_j}(\Delta_j\rho)\right)\frac{u_i|_{(m\pm1)}u_i|_{(m)}}{2} + \left(-\beta^*_{m\pm\frac{1}{2}}\widehat{\frac{\partial u_k}{\partial x_k}}|_{(m\pm\frac{1}{2})}\delta_{ij}\right)\bar{u}_i^{(m\pm\frac{1}{2})}, \tag{5.6}$$

$$\hat{I}_j^d|_{(m\pm\frac{1}{2})} = -\frac{D^*_{m\pm\frac{1}{2}}}{\Delta x_j}\Delta_j(\rho e), \tag{5.7}$$

$$\tag{5.8}$$

where $\hat{C}_j^d|_{(m\pm1/2)}$, $\hat{M}_{ij}^d|_{(m\pm1/2)}$, $\hat{K}_j^d|_{(m\pm1/2)}$, and $\hat{I}_j^d|_{(m\pm1/2)}$ are the localized LF-type total dissipative fluxes of mass, momentum, kinetic energy, and internal energy, respectively.

6. Results

In this section, the proposed artificial-viscosity method is used to simulate a wide variety of test cases, involving the classical one-dimensional shock-tube case and an LES of compressible turbulent flow, to assess the accuracy of this method in capturing the discontinuities as well as its low-dissipative nature and robustness in simulating compressible turbulent flows. The proposed method is implemented in the low-dissipative CTR-DIs3D solver (Jain *et al.* 2020; Jain & Moin 2020), which uses a second-order central scheme and a fourth-order Runge-Kutta scheme for spatial and temporal discretizations, respectively.

6.1. *Modified Sod test case*

The modified Sod-shock tube is a classic one-dimensional test case used to assess the accuracy of shock and contact discontinuity-capturing methods that was originally proposed by Sod (1978). Here, a modified version of the test case is used, because an entropy-consistent scheme is needed to avoid the entropy-violating jump that would otherwise form in the expansion region of this modified Sod shock-tube case (Chandrashekar 2013). The initial setup consists of a Riemann problem with the left state

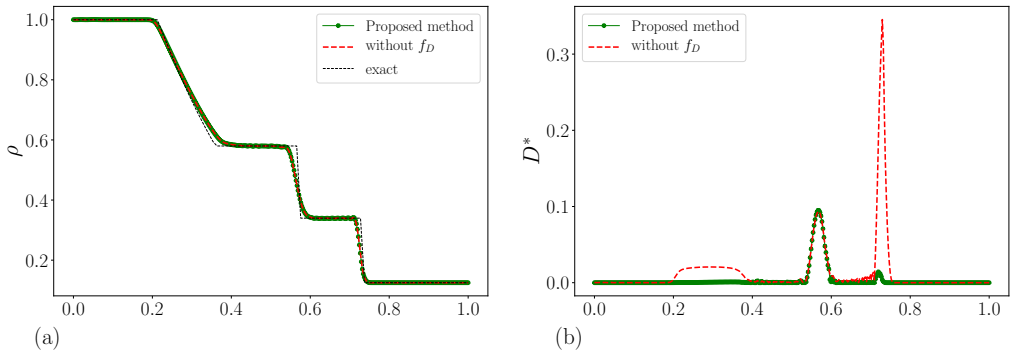

FIGURE 1. Modified version of the Sod shock-tube test case: (a) density, ρ, and (b) artificial mass diffusivity, D^*.

$(\rho, u, p) = (1.0, 0.75, 1.0)$ and the right state $(\rho, u, p) = (0.125, 0.0, 0.1)$, and the discontinuity located at $x = 0.3$. Here, $N = 400$ is the number of grid points, and the results are presented at the final time of $t = 0.2$ in Figure 1.

The simulation results in Figure 1 show that the shock and contact discontinuities are captured accurately with the proposed EC-LAD method, and that the method does not suffer from the formation of entropy-violating shock. The density, ρ, and artificial mass diffusivity, D^*, are plotted in Figure 1(a) and 1(b), respectively, at time $t = 0.2$, with and without the newly proposed switching sensor, f_D. Figure 1(b) shows that the D^* is active around the shock, contact discontinuity, and expansion fan when the proposed f_D sensor is not being used. However, the use of the f_D sensor localizes D^* mostly to regions around the contact discontinuity. Non-zero values of D^* around shocks would unnecessarily make the method more dissipative because β^* is already active in this region to resolve the shock. Therefore, the use of the new switching sensor f_D makes the method less dissipative without affecting the accuracy of the solution.

6.2. *Decaying homogeneous isotropic turbulence with shocklets*

In this section, the non-dissipative nature, accuracy, and robustness of the proposed artificial-viscosity method are assessed for the LES of compressible turbulent flows with shocklets. Here, a decaying homogeneous isotropic turbulence (HIT) is simulated at a high enough Mach number that shocklets are generated in the flow (Lee *et al.* 1991). The initial Taylor-scale Reynolds number of the flow is $Re_{\lambda,o} = 100$, and the turbulent Mach number is $M_{t,o} = 0.6$. The Prandtl number is chosen to be $Pr = 0.7$, and the material properties of the fluid are $\gamma = 1.4$ and $R = 1$. The domain is triply periodic cube with dimensions $[0, 2\pi]$. Here, a coarse resolution of 64^3 grid points is used, and hence, this is a good test to assess the amount of numerical dissipation added by the shock- and contact discontinuity-capturing method.

Figure 2 shows the results from the simulation (a) with f_D and f_β (the proposed method), (b) with f_D and without f_β, (c) without f_D and with f_β, and (d) without f_D and without f_β. To compare the results, a direct numerical simulation (DNS) of the same test case is performed on a 256^3 mesh; the results are also filtered onto a 64^3 mesh and are shown in Figure 2. Clearly, the simulation results show that the use of f_D and f_β sensors is necessary to recover the correct dilatational, density, and vorticity variances.

The simulations are the least accurate without the use of the f_D and f_β sensors. Using these f_D and f_β sensors individually improves the results by making the method

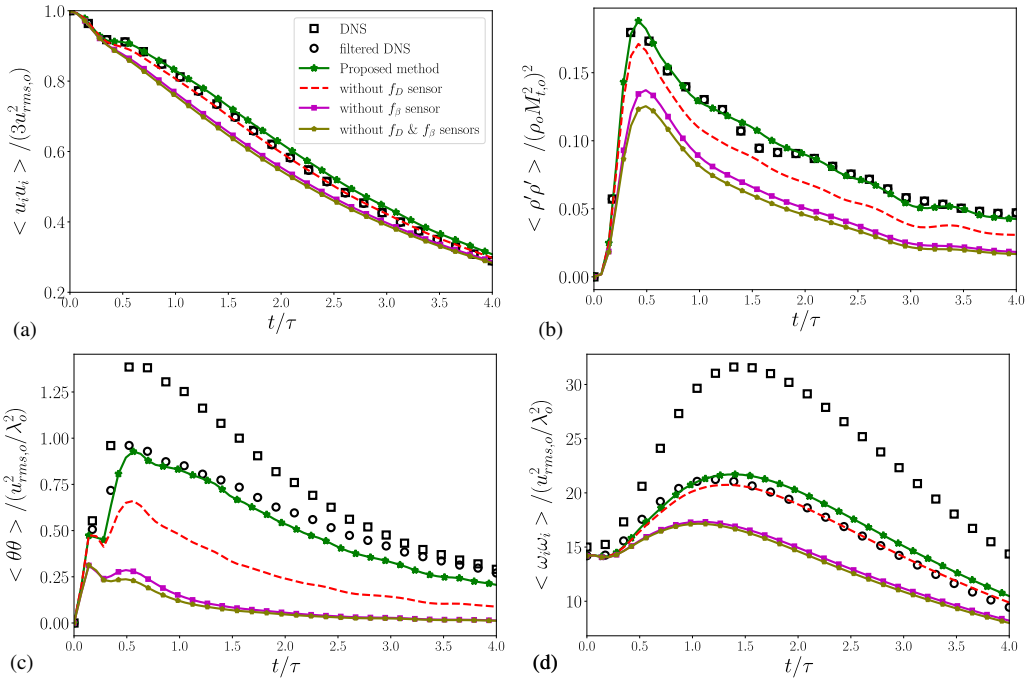

FIGURE 2. Simulation of decaying HIT with shocklets at $M_{to} = 0.6$. (a) Mean square velocity, (b) density variance, (c) dilatational variance, and (d) vorticity variance.

less dissipative, and using both sensors gives the best results. Therefore, the proposed method along with the sensors results in a robust, accurate, and low-dissipative method for capturing shocks and contact discontinuities for LES of compressible turbulent flows.

6.3. *Shock-vortex interaction*

In this section, a shock-vortex interaction is simulated using the proposed artificial-viscosity method. Section 6.2 demonstrated that the proposed method is low-dissipative and is suitable for LES of compressible turbulent flows. This section, in contrast, will assess the accuracy and suitability of the present method for the DNS of compressible turbulent flows.

This test case is taken from the work of Inoue & Hattori (1999), Zhang *et al.* (2005), and Chatterjee & Vijayaraj (2008) and has also been used to evaluate the shock-capturing capability by Subramaniam *et al.* (2019) and Haga & Kawai (2019). The initial setup of this case consists of a $M = 1.2$ stationary shock located at $x = 0$ and an isentropic vortex of strength $M_v = 0.25$, initially located upstream of the shock at $x = 4$. The initial vortex field is given by

$$u_\theta(r) = M_v r \exp\left(\frac{1-r^2}{2}\right), \quad u_r(r) = 0, \tag{6.1}$$

$$p(r) = \frac{1}{\gamma}\left[1 - \left(\frac{\gamma-1}{2}\right) M_v^2 \exp\left(1-r^2\right)\right]^{\frac{\gamma}{\gamma-1}}, \tag{6.2}$$

$$\rho(r) = \left[1 - \left(\frac{\gamma-1}{2}\right) M_v^2 \exp\left(1-r^2\right)\right]^{\frac{1}{\gamma-1}}, \tag{6.3}$$

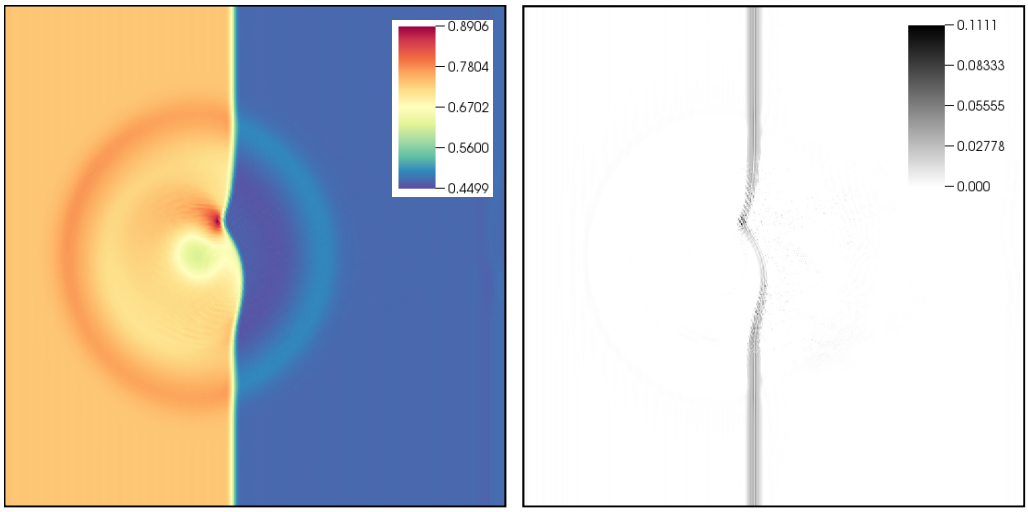

FIGURE 3. (a) The pressure field, p, and (b) the artificial bulk viscosity, β^*, for the case of shock-vortex interaction at $t = 6$.

where u_θ is the angular velocity, u_r is the radial velocity, r is the radial distance from the center of the vortex, and γ is the ratio of specific heats. The pressure field at the time of $t = 6$ is shown in Figure 3 along with the ABV, β^*. At this time, the vortex has passed through the shock and generates a deformed shock surface. The results show that the f_β sensor has successfully localized β^* only to those regions around the shock, while maintaining the accuracy in capturing the shock without the need for separately tuning the coefficients in this case.

7. Conclusions

In this work, we propose a novel, entropy-consistent, and stable LAD-based shock- and contact discontinuity-capturing method. Using an analogy between the LF flux and the artificial-viscosity methods, a discrete LF-type flux formulation is presented for the proposed LAD method. The proposed method satisfies the discrete kinetic energy– and entropy-consistency conditions presented by Jain & Moin (2020), hence the name. We use a modified Ducros sensor that further localizes the artificial bulk viscosity, and we propose a new switching sensor that localizes the artificial mass/thermal diffusivity that is responsible for capturing contact discontinuities. These sensors are designed in a way that the resulting method does not require tuning coefficients, depending on the problem being solved, that are typical of classical LAD methods. We show that the proposed method accurately captures shocks and contact discontinuities, without the need for problem-dependent tuning, for a wide range of problems, such as the one-dimensional Sod test case, decaying HIT with shocklets, and shock-vortex interaction. Therefore, the proposed method is suitable for LES and DNS of compressible turbulent flows with discontinuities. An extension of the proposed method to compressible two-phase flows is presented in the Appendix.

Acknowledgments

S. S. J. acknowledges support from the Franklin P. and Caroline M. Johnson Graduate Fellowship. P.M. acknowledges support from the Predictive Science Academic Alliance Program (PSAAP-III) Center at Stanford University. S. S. J. thanks Mr. Tim Flint for providing helpful comments on the brief and for helping with the exact solution of the Sod shock-tube test case.

Appendix. Extension to two-phase flows

For the simulation of two-phase flows, we use the five-equation model of Allaire *et al.* (2002) and Kapila *et al.* (2001) with the conservative diffuse-interface method for compressible two-phase flows (Jain *et al.* 2020; Jain & Moin 2020). Following Section 3, the proposed artificial-viscosity method for two-phase flows with this five-equation diffuse-interface model can be written as

$$\frac{\partial \phi_1}{\partial t} + \frac{\partial u_j \phi_1}{\partial x_j} = (\phi_1 + \zeta_1)\frac{\partial u_j}{\partial x_j} + \frac{\partial a_{1j}}{\partial x_j} + \frac{\partial}{\partial x_j}\left(D^* \frac{\partial \phi_l}{\partial x_j}\right), \tag{7.1}$$

$$\frac{\partial \rho_l \phi_l}{\partial t} + \frac{\partial u_j \rho_l \phi_l}{\partial x_j} = \frac{\partial R_{lj}}{\partial x_j} + \frac{\partial}{\partial x_j}\left(D^* \frac{\partial \rho_l \phi_l}{\partial x_j}\right), \qquad l = 1, 2, \tag{7.2}$$

$$\begin{aligned} \frac{\partial \rho u_i}{\partial t} + \frac{\partial \rho u_i u_j}{\partial x_j} + \frac{\partial p}{\partial x_i} = \frac{\partial u_i f_j}{\partial x_j} + \frac{\partial \tau_{ij}}{\partial x_j} + \sigma\kappa\frac{\partial \phi_1}{\partial x_i} + \rho g_i \\ + \frac{\partial}{\partial x_j}\left(D^* u_i \frac{\partial \rho}{\partial x_j}\right) + \frac{\partial}{\partial x_j}\left(\beta^* \frac{\partial u_k}{\partial x_k}\delta_{ij}\right), \end{aligned} \tag{7.3}$$

$$\begin{aligned} \frac{\partial E}{\partial t} + \frac{\partial \left(E + p\right) u_j}{\partial x_j} = \frac{\partial \tau_{ij} u_i}{\partial x_j} + \frac{\partial k f_j}{\partial x_j} + \sum_{l=1}^{2} \frac{\partial \rho_l h_l a_{lj}}{\partial x_j} + \sigma\kappa u_i \frac{\partial \phi_1}{\partial x_i} + \rho u_i g_i \\ + \frac{\partial}{\partial x_j}\left[D^* \frac{\partial \rho}{\partial x_j}\left(\frac{u_k u_k}{2}\right)\right] + \frac{\partial}{\partial x_j}\left(D^* \frac{\partial \rho e}{\partial x_j}\right) + \frac{\partial}{\partial x_j}\left(\beta^* \frac{\partial u_k}{\partial x_k}\delta_{ij} u_i\right), \end{aligned} \tag{7.4}$$

where ϕ_l is the volume fraction of phase l that satisfies the condition $\sum_{l=1}^{2} \phi_l = 1$; ρ_l is the density of phase l; ρ is the total density, defined as $\rho = \sum_{l=1}^{2} \rho_l \phi_l$; $\vec{u}$ is the velocity; p is the pressure; e is the specific mixture internal energy, which can be related to the specific internal energy of phase l, e_l, as $e = \sum_{l=1}^{2} \rho_l e_l$; $k = u_i u_i / 2$ is the specific kinetic energy; $E = \rho(e + k)$ is the total energy of the mixture per unit volume; and the function ζ_1 is given by

$$\zeta_1 = \frac{\rho_2 c_2^2 - \rho_1 c_1^2}{\frac{\rho_1 c_1^2}{\phi_1} + \frac{\rho_2 c_2^2}{\phi_2}}, \tag{7.5}$$

where c_l is the speed of sound for phase l. In Eq. (7.4), $h_l = e_l + p/\rho_l$ represents the specific enthalpy of phase l and can be expressed in terms of ρ_l and p using the stiffened-gas equation of state as

$$h_l = \frac{(p + \pi_l)\gamma_l}{\rho_l(\gamma_l - 1)}. \tag{7.6}$$

In Eqs. (7.1)-(7.4), σ is the surface-tension coefficient, $\kappa = -\vec{\nabla} \cdot \vec{n}_1$ is the curvature of the interface, $\vec{g}$ is the gravitational acceleration, and $\vec{a}_l$ is the volumetric interface-regularization flux for phase l, which satisfies the condition $\vec{a}(\phi_1) = -\vec{a}(\phi_2)$. $\vec{n}_l =$

$\vec{\nabla}\phi_l/|\vec{\nabla}\phi_l|$ is the normal of the interface for phase l; $\vec{R}_l = \rho_l \vec{a}_l$ is the interface-regularization flux in the mass balance equation for phase l. $\vec{f} = \sum_{l=1}^{2} \vec{R}_l = \sum_{l=1}^{2} \rho_l \vec{a}_l$ is the net interface-regularization flux for the mixture mass. Note that the artificial diffusivities in Eqs. (3.7) and (3.8) work well for two-phase flows with minimal modifications (not included here for brevity).

REFERENCES

Adler, M. C. & Lele, S. K. 2019 Strain-hardening framework for Eulerian simulations of multi-material elasto-plastic deformation. In *Annual Research Briefs,* Center for Turbulence Research, Stanford University, pp. 257-271.

Allaire, G., Clerc, S. & Kokh, S. 2002 A five-equation model for the simulation of interfaces between compressible fluids. *J. Comput. Phys.* **181**, 577–616.

Aslani, M. & Regele, J. D. 2018 A localized artificial diffusivity method to simulate compressible multiphase flows using the stiffened gas equation of state. *Int. J. Numer. Methods Fluids* **88**, 413–433.

Bhagatwala, A. & Lele, S. K. 2009 A modified artificial viscosity approach for compressible turbulence simulations. *J. Comput. Phys.* **228**, 4965–4969.

Chandrashekar, P. 2013 Kinetic energy preserving and entropy stable finite volume schemes for compressible Euler and Navier-Stokes equations. *Comput. Phys. Commun.* **14**, 1252–1286.

Chatterjee, A. & Vijayaraj, S. 2008 Multiple sound generation in interaction of shock wave with strong vortex. *AIAA J.* **46**, 2558–2567.

Cook, A. W. 2007 Artificial fluid properties for large-eddy simulation of compressible turbulent mixing. *Phys. Fluids* **19**, 055103.

Ducros, F., Ferrand, V., Nicoud, F., Weber, C., Darracq, D., Gacherieu, C. & Poinsot, T. 1999 Large-eddy simulation of the shock/turbulence interaction. *J. Comput. Phys.* **152**, 517–549.

Germano, M., Piomelli, U., Moin, P. & Cabot, W. H. 1991 A dynamic subgrid-scale eddy viscosity model. *Phys. Fluids* **3**, 1760–1765.

Haga, T. & Kawai, S. 2019 On a robust and accurate localized artificial diffusivity scheme for the high-order flux-reconstruction method. *J. Comput. Phys.* **376**, 534–563.

Inoue, O. & Hattori, Y. 1999 Sound generation by shock–vortex interactions. *J. Fluid Mech.* **380**, 81–116.

Jain, S. S., Adler, M. C., West, J. R., Mani, A., Moin, P. & Lele, S. K. 2021 Assessment of diffuse-interface methods for compressible multiphase fluid flows and elastic-plastic deformation in solids. *Arxiv preprint #2109.09729*.

Jain, S. S., Mani, A. & Moin, P. 2020 A conservative diffuse-interface method for compressible two-phase flows. *J. Comput. Phys.* **418**, 109606.

Jain, S. S. & Moin, P. 2020 A kinetic energy and entropy preserving scheme for the simulation of compressible two-phase turbulent flows. *Annual Research Briefs*, Center for Turbulence Research, Stanford University, pp. 299-312.

Kapila, A., Menikoff, R., Bdzil, J., Son, S. & Stewart, D. S. 2001 Two-phase modeling of deflagration-to-detonation transition in granular materials: Reduced equations. *Phys. Fluids* **13**, 3002–3024.

Kawai, S. & Lele, S. K. 2008 Localized artificial diffusivity scheme for discontinuity capturing on curvilinear meshes. *J. Comput. Phys.* **227**, 9498–9526.

Kawai, S., Shankar, S. K. & Lele, S. K. 2010 Assessment of localized artificial diffusivity scheme for large-eddy simulation of compressible turbulent flows. *J. Comput. Phys.* **229**, 1739–1762.

Lee, C. Y. & Lele, S. K. 2017 Localized artificial diffusivity scheme for deflagrations and detonation waves. *Comput. Fluids* **159**, 33–52.

Lee, S., Lele, S. K. & Moin, P. 1991 Eddy shocklets in decaying compressible turbulence. *Phys. Fluids* **3**, 657–664.

LeVeque, R. J. 1992 *Numerical Methods for Conservation Laws*, vol. 132. Springer.

Mani, A., Larsson, J. & Moin, P. 2009 Suitability of artificial bulk viscosity for large-eddy simulation of turbulent flows with shocks. *J. Comput. Phys.* **228**, 7368–7374.

Sod, G. A. 1978 A survey of several finite difference methods for systems of nonlinear hyperbolic conservation laws. *J. Comput. Phys.* **27**, 1–31.

Subramaniam, A., Ghaisas, N. S. & Lele, S. K. 2018 High-order Eulerian simulations of multimaterial elastic–plastic flow. *J. Fluids Eng.* **140**, 050904.

Subramaniam, A., Wong, M. L. & Lele, S. K. 2019 A high-order weighted compact high resolution scheme with boundary closures for compressible turbulent flows with shocks. *J. Comput. Phys.* **397**, 108822.

Zhang, S., Zhang, Y.-T. & Shu, C.-W. 2005 Multistage interaction of a shock wave and a strong vortex. *Phys. Fluids* **17**, 116101.